Quim. Nova, Vol. 35, No. 9, 1724-1727, 2012

Artigo

A COMPARATIVE STUDY OF HYDROXYAPATITE NANOPARTICLES SYNTHESIZED BY DIFFERENT ROUTES

Adrian Paz*, Dainelys Guadarrama, Mónica López, Jesús E. González, Nayrim Brizuela and Javier Aragón
Biomaterials and Nanostructures Group, National Center for Scientific Research, 25 Ave. and 158st, Havana, Cuba

Recebido em 15/11/11; aceito em 18/5/12; publicado na web em 24/8/12

In this study, bioactive hydroxyapatite nanoparticles were prepared by two different methods: wet chemical precipitation and biomimetic precipitation. The aim was to evaluate the morphology, particle-size, crystallinity and phases of the powders obtained by traditional wet chemical precipitation and the novel biomimetic precipitation using a supersaturated calcium solution. The nanoparticles were investigated by transmission electron microscopy, Fourier transform infrared spectroscopy and X-ray diffraction. The results revealed that the nanoparticles were formed by hydroxyapatite with a high crystallinity and controlled morphology. Additionally, it was found that the shape and size of the nanoparticles can be modified with each preparation method.

Keywords: hydroxyapatite nanoparticles; wet chemical precipitation; biomimetic precipitation.

INTRODUCTION

Bioactive materials based on hydroxyapatite nanoparticles (HAn, $Ca_{10}(PO_4)_6(OH)_2$) have been widely used in the biomedical field, as implant materials for bone tissue substitution, in drug delivery systems and for many other applications, due to their high biocompatibility and surface active properties.[1-3] In addition, HAn has been developed to improve adsorption and photocatalytic decomposition activity against toxic metals, bacteria, viruses and other biohazardous substances.[4,5] In recent years, several chemistry-based processing routes have been reported for preparing HAn powders. Nanoparticles with several morphologies have been synthesized by means of solid-state reaction, the emulsion technique, sol-gel and the hydrothermal method.[6-11] However, the wet chemical precipitation method was proven to be one of the easiest ways of preparing HAn powders. Akao *et al*.[10] prepared HAn nanocrystals based on the following reaction of calcium hydroxide ($Ca(OH)_2$) with orthophosphoric acid (H_3PO_4):

$$10\ Ca(OH)_2 + 6\ H_3PO_4 \rightarrow Ca_{10}(PO_4)_6(OH)_2 + 18H_2O \quad (1)$$

The morphology (shape and size) of the nanoparticles obtained by this method is very sensitive to the reactant addition rate, as well as to temperature and pH.[11] Another interesting and low-cost method of synthesis is by preparing HAn in metastable synthetic body fluid (SBF) under "biomimetic" conditions (37 °C and pH 7.4). Tas *et al*.[12] reported the formation of HAn by the biomimetic method in 24 h, with controlled morphology and a high degree of phase purity. Recently, supersaturated calcium solutions (SCS) containing inorganic ions in higher concentrations than their counterparts present in SBF, have become the most used solutions in bioceramics applications due to the shorter process time.[13,14] This study focuses on the characteristics of the HAn powders synthesized by two different routes: the traditional wet chemical precipitation and the novel biomimetic precipitation using SCS solutions.

EXPERIMENTAL

Biomimetic precipitation (HAn1)

For the preparation of the supersaturated calcium solution, 0.555 g of calcium chloride ($CaCl_2$), 0.150 g of sodium dihydrogen phosphate (NaH_2PO_4) and 0.073 g of sodium bicarbonate ($NaHCO_3$) were dissolved in 500 mL of distilled water. The solution was stirred at 80 rpm and the temperature adjusted to 37 °C for 24 h. At the end of the process, the precipitate was washed with deionized water and dried in an oven at 110 °C for 2 h.

Wet chemical precipitation (HAn2)

In this method of synthesis, 100 mL of 0.3 M H_3PO_4 solution was added to an equal volume of 0.5 M $Ca(OH)_2$ solution at a drip rate of two drops per second, at room temperature. The pH value was kept above 10 by the addition of ammonium hydroxide (NH_4OH) during the precipitation process. The resultant precipitate was left in the mother solution for 5 days and finally was washed and dried using the same procedure employed for the biomimetic precipitation.

Physical, chemical and morphological characterization

The typical groups of the synthesized powders were analyzed by Fourier transform infrared spectroscopy (FT-IR, Model Thermo Nicolet´s Avatar), in the wave number range of 400-4000 cm^{-1}, with a resolution of 4 cm^{-1}.

X-ray powder diffraction (XRPD) studies were carried out on a ThermoARL XTRA powder diffractometer, using Bragg-Brentano geometry with Cu Kα radiation and a solid-state Peltier cooled detector. All powder diffraction patterns were measured in continuous mode using the following conditions: 2θ angular range 20-60°, tube power 45 kV and 40 mA, 2θ step size 0.02° using a scan rate of 1° 2θ/min. The diffraction patterns were compared with those in the Powder Diffraction Files (PDF) database of the Joint Committee on Powder Diffraction Standards (JCPDS).

The phase analysis was performed by a Rietveld analysis of both synthesized powders, using the TOPAS-Academic V3.1 software. The starting model used in the Rietveld refinement was based on the structures reported in the literature, reference for hydroxyapatite (American Mineralogist Crystal Structure Database code # 0001257).[15] The background was fitted with an 18-parameter Chebychev polynomial function and the instrumental profile parameters, fitted from the Corundum standard, were kept fixed.

The crystallinity degree (Xc) of the HAn was determined using Equation 2:[16]

*e-mail: adrianpazramos@yahoo.es

$$X_c = \left(\frac{0.24}{\beta}\right)^3 \cdot 100\% \quad (2)$$

where β is the FWHM (rad) and θ is Bragg's diffraction angle (°).

The morphology and size distribution of the synthesized HAn powders was characterized with a transmission electron microscope (TEM, Model Philips CM10), operating at 80 kV and a particle size analyzer (ImageJ), respectively.

RESULTS AND DISCUSSION

FT-IR and XRD results

The infrared spectra of the synthesized powders are given in Figure 1. The characteristic bands of internal phosphate (PO_4^{3-}) mode were assignments in both spectra: the band at 472 cm^{-1} was assigned to ν_2 (OPO) bending mode; the presence of two characteristic bands around 568 and 601 cm^{-1} correspond to ν_4 (OPO) bending mode; the 960 cm^{-1} band in the spectra was assigned to ν_1 (PO) symmetric stretching and the doublet in the range 1100-1000 cm^{-1} was assigned to ν_3 (PO) antisymmetric stretching mode. These bands indicate the characteristic molecular structures of the polyhedrons of PO_4^{3-} in the apatite lattice.[17] Further, at 3572 cm^{-1} the main hydroxyl vibration ν (OH^-) was observed in both spectra; in HAn1 spectrum a band at 635 cm^{-1} was observed, which is attributed to OH^- groups (δ),[17] yet is not observed in the HAn2 spectrum. On the other hand, the observed bands at 3400 and 1640 cm^{-1} (H_2O) in both spectra, correspond to water absorption during the synthesis process.

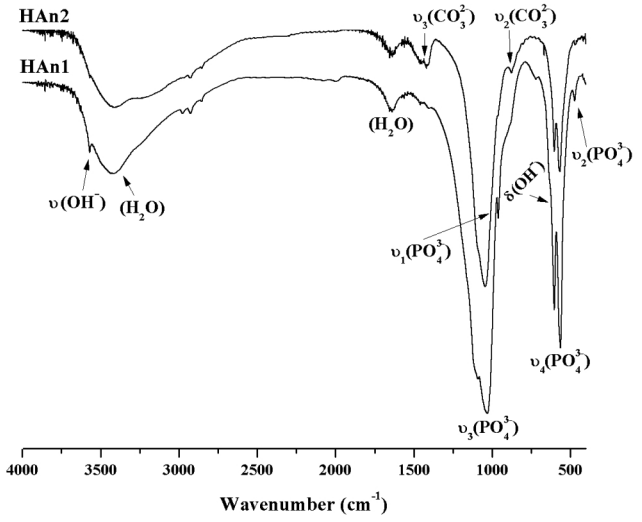

Figure 1. *Typical FT-IR spectra of the precipitated powders*

The FT-IR spectrum of the HAn2 obtained by wet chemical precipitation shows carbonate peaks in the range 1500-1400 and 868 cm^{-1}, corresponding to the asymmetric stretching (ν_3 mode) and out--of-plane bending (ν_2 mode) vibrations, respectively.[18] The formation of carbonate is due to the adsorption of atmospheric CO_2 during the ripening time. This phenomenon is related to the highly alkaline conditions in the solution, in which there are sufficient OH^- ions for the reaction with CO_2.[19,20]

X-ray diffraction analyses were employed to confirm the crystalline phase formation, degree of crystallinity and crystallite size of the powders synthesized by the two methods (Figure 2).

Figure 2 shows the XRPD patterns of the powders synthesized compared with the reference pattern of JCPDS: PDF Ref. 09-0432. The diffraction peaks correspond to those of hexagonal synthetic

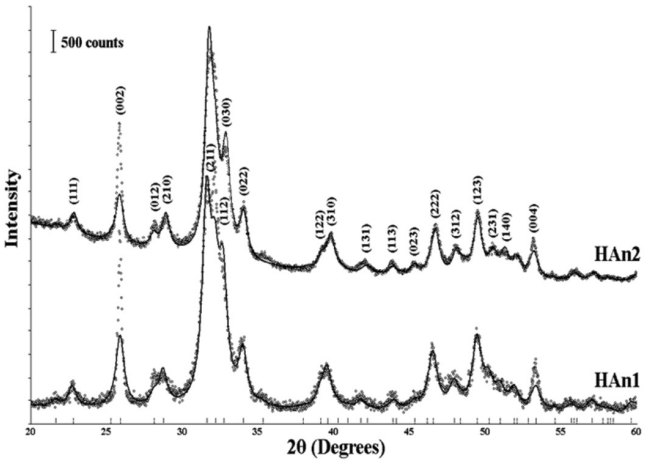

Figure 2. *Experimental (dash point) and calculated XRPD patterns (solid lines) of the precipitated powders*

hydroxyapatite and space group P63/m.

The peak broadening reflects the nanocrystalline nature of the synthesized powders. Table 1 shows the results of Rietveld analysis and gives the lattice parameters and crystal size of HAn1 and HAn2. The apparent size of HAn crystallites obtained from XRPD patterns analysis is similar for both HAn obtained.

Table 1. Results of Rietveld refinement of both HAn

Sample	PDF Ref. 74-0566	HAn1	HAn2
R_{wp}	---	15.377	6.037
a=b (Å)	9.424	9.472 (3)	9.421 (3)
c (Å)	6.879	6.658 (2)	6.881 (2)
Cristal Size (nm)	---	14.7 (2)	16.1 (2)
R_{Bragg}	---	3.475	2.806

The HAn crystallites are approximately 14.7 ± 0.2 and 16.1 ± 0.2 nm in length for HAn1 and HAn2, respectively. These values are slightly lower than the range reported for bone apatite crystallites (20-40 nm in length).[21] The anisotropic crystallites are significantly longer in the c-direction than in the a- or b-directions. The crystallites consistently share these dimensions regardless of the mass of HAn. This geometry mimics actual bone apatite crystals which are anisotropic and elongated along the c-axis.[22]

The evaluated degrees of crystallinity for HAn1 and HAn2 powders were 67 and 42%, respectively. This result shows a higher crystallinity for the nanohydroxyapatite obtained by the biomimetic method in only 24 h.

TEM and particle size distribution results

The morphologies of the nanoparticles prepared by the two different routes are shown in Figure 3. The HAn powders obtained by the biomimetic precipitation method (HAn1) were spherical or close to spherical in shape, with an average diameter of 27 ± 5 nm. On the other hand, the particles synthesized by the wet chemical precipitation method (HAn2), showed needle-like morphology with a particle width of 62 ± 22 nm and length of 23 ± 7 nm. In both cases, the particles showed a high tendency to agglomerate. This result is due to the increasing of the ripening time that cause the preferential growth orientation observed along the plane formed by the calcium1 atoms (002) inside the hydroxyapatite crystal.

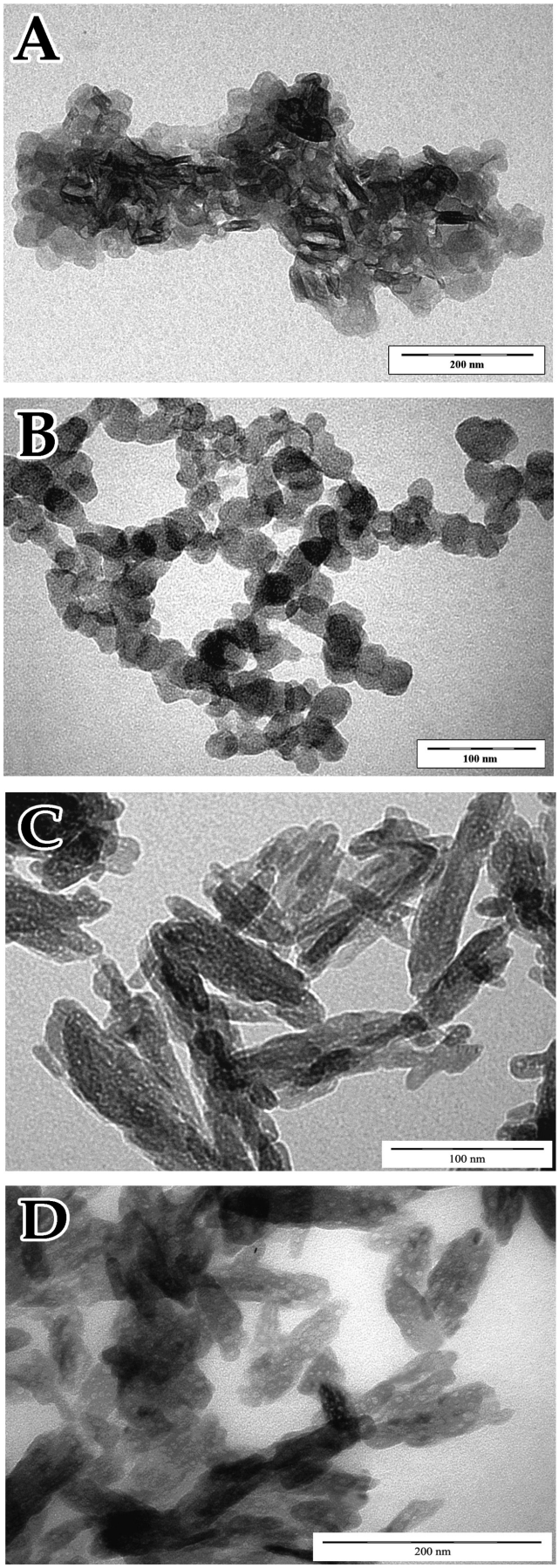

Figure 3. *TEM micrographs of the particles precipitated in solutions. A - B: HAn1, C - D: HAn2*

Figure 4 shows the particle size distribution of HAn samples which are synthesized by biomimetic and wet chemical precipitation methods.

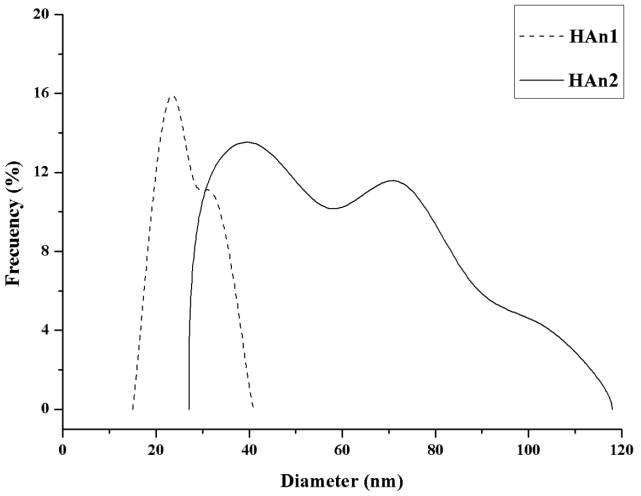

Figure 4. *Particle size distributions of HAn powders*

As seen in the figure, the particle size distributions obtained by both synthesis methods are quite different. In terms of particle distribution, the ranges were within 15-41 nm for the particles obtained by biomimetic precipitation and 27-118 nm for the samples produced according to wet chemical precipitation.

The morphology and crystallinity of the precipitated powder proved closely related with the exposure time in the solutions (ripening time). The decrease in crystallinity with the increase in ripening time was observed clearly by the sharpening of the diffraction peaks of the HAn powders (Figure 2) (Table 2).

Table 2. Characteristics of the HAn powders

Sample	Particle size (nm)	Crystallite size (nm)	Degree of crystallinity (%)
HAn1	27 (5)	14.7 (2)	67
HAn2	62 (22)	16.1 (2)	42

Hydroxyapatite formation from metastable aqueous solutions is usually preceded by a precursor phase, most commonly amorphous calcium phosphate (ACP) or octacalcium phosphate (OCP). The precursor calcium phosphate then hydrolyzes into the more thermodynamically stable hydroxyapatite. The precursor phase depends on the conditions present in the solution during the precipitation reaction.[23] The presence of the PO_4^{3-} doublet at 601 and 568 cm^{-1} in spectra suggests that the precursor phase of HAn1 and HAn2 was OCP (Figure 1).[23]

In the formation of OCP, Ca^{2+} ions first complexes with another species before combining with phosphate. By ordering the calcium cations onto a matrix prior to mineralization, the OCP precursor ensures a more crystalline and ordered HA phase.[24] The thermodynamically unstable OCP then hydrolyzes into a crystalline HA phase which is confirmed by Rietveld analysis.

Figure 5 shows the behavior of the pH values during the biomimetic process.

The initial pH value of the solution was measured as 6.35 and increased to a maximum of 6.52 within the first hour of the process. This rapid augmentation in pH values was due to the reaction of hydrogen carbonate ions (HCO_3^-) with the H^+ ions from the solution, to form CO_2 and water, as follows:

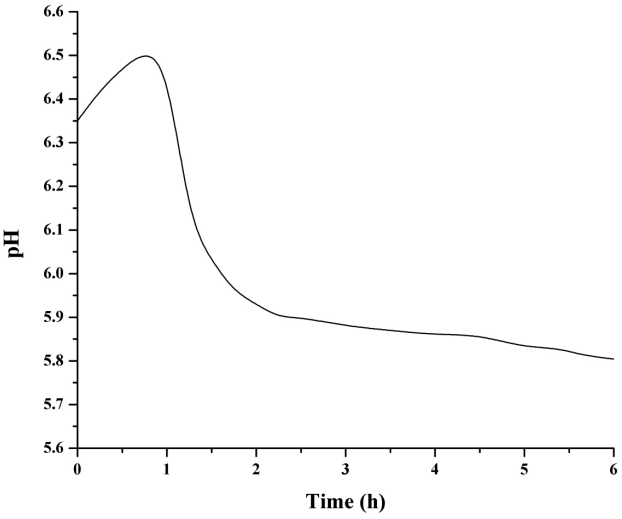

Figure 5. *pH evolution curve of the SCS solution*

$$H^+ + HCO_3^- \rightarrow CO_2 \uparrow + H_2O \quad (3)$$

The second step of the biomimetic precipitation occurs between the first and second hours of the process and is related with the formation of the HA crystal seeds in the solution, which cause the rapid consumption of hydroxide (OH^-) groups by reaction 4:

$$10\ Ca^{2+} + 6\ PO_4^{3-} + 2\ OH^- \rightarrow Ca_{10}(PO_4)_6(OH)_2 \downarrow \quad (4)$$

The pH values decreased slowly from two hours to the end of the process at 24 h, which indicates that the growing of the HA nanoparticles occurred very slowly (Figure 5).

HA is the most stable compound of calcium phosphate phases in aqueous solution at pH values higher than 4.2.[12] However, the synthesis of this compound is usually carried out in a highly alkaline media (up to pH 10) to ensure the phase purity of the product formed. We can conclude that biomimetic precipitation using SCS solutions allows the obtention of HA nanoparticles with high purity, controlled morphology and nanometric size, in slightly acidic solutions.

CONCLUSIONS

Both biomimetic and wet chemical precipitation represent simple, fast and economic routes for the synthesis of hydroxyapatite nanoparticles. The morphology and crystallinity of the resulting nanoparticles are dependent on the synthesis method and ripening time. In the HAn obtained by the wet chemical and the biomimetic precipitation method, the precursor phase was OCP and within the hydroxyapatite crystal a preferential growth along the plane formed by calcium1 atoms (002) was observed. The HAn particles obtained show different morphology depending on the synthesis method, where HAn1 and HAn2 showed spherical and needle-like morphologies, respectively.

REFERENCES

1. Ganesan-Balasundarama, M. S.; Webster, T. J.; *Biomaterials* **2006**, *27*, 2798.
2. Viswanath, B.; *Biomaterials* **2008**, *29*, 4855.
3. Dorozhkin, S. V.; *Acta Biomaterialia* **2010**, *6*, 715.
4. Yang, Z.; Gong, X.; Zhang, C.; *Chem. Eng. J*. **2010**, *165*, 117.
5. Vojislav-Stanica, S. D.; Jelena, A.; Miodrag, M.; Bojan, J.; Ilija, B.; Plecas, S. R.; *Appl. Surf. Sci*. **2010**, *256*, 6083.
6. Hu, X. J.; Liu, J.; Lu, K.; Mu, Y. J.; *Mater. Lett*. **2008**, *62*, 3824.
7. Manuel, A.; Martins, C. S.; Maria, M. A.; Maria, E. V. C.; *J. Colloid Interface Sci*. **2008**, *318*, 210.
8. Ferraz, M. P.; Manuel, C. M.; *J. Applied Biomaterials and Biomechanics* **2004**, *2*, 74.
9. Zhang, K. C.; Zhi You, L.; Su Ping, H.; *J. Phys. Chem. Solids* **2009**, *70*, 243.
10. Akao, M.; Aoki, H.; Kato, K.; *J. Mater. Sci.* **1981**, *16*, 809.
11. Wang, P.; *Powder Technol*. **2010**, *203*, 315.
12. Cüneyt Tas, A.; *Biomaterial* **2000**, *21*, 1429.
13. Li, F.; Feng, Q. L.; Cui, F. Z.; Li, H. D.; Schubert, H.; *Surf. Coat. Technol*. **2002**, *154*, 88.
14. Ciobanu, G.; Carja, G.; Ciobanu, O.; Sandu, I.; Sandu, A.; *Micron* **2009**, *40*, 143.
15. Nebahat-Degirmenbasi, D. M. K.; Elvan, B.; *Colloids Surf, B* **2006**, *48*, 42.
16. Fowler, B. O.; *Inorg. Chem*. **1974**, *13*, 194.
17. Gen-Tao, Z.; Qi-Zhi, Y.; Jie, N.; Gu, J.; *Am. Mineral*. **2009**, *94*, 293.
18. Iryna-Sporysh, E. S.; Oleg, L.; Shynkaruk, A.; Vitalii-Dubok, E. B.; Uwe, R.; Scharff, P.; *Mater. Sci. Eng., B* **2010**, *169*, 128.
19. Muller, L.; Caillard, D.; Muller, F. A.; *Biomolecular Engineering* **2007**, *24*, 462.
20. Hughes, J. M.; Cameron, M.; Crowley, K. D.; *Am. Mineral*. **1989**, *74*, 870.
21. Park, J. B.; *Biomaterials Science and Engineering,* Plenum Publishing: New York, 1984.
22. Danilchenko, S. N.; Moseke, C.; Sukhodub, L. F.; Sulkio-Cleff, B.; *Cryst. Res. Technol*. **2004**, *39*, 71.
23. Sauer, G. R.; Wuthier, R. E.; *J. Biol. Chem*. **1988**, *27*, 13718.
24. Hutchens, S.; Benson, R.; Evans, B.; O'Neill, H.; Rawn, C.; *Biomaterials* **2006**, *27*, 4661.